International Journal of Engineering, Management, Humanities and Social Sciences Paradigms (Volume 31, Special Issue of January 2019)
ISSN (Online): 2347-601X and Website: www.ijemhs.com

# MASCA-PSO based LLRBFNN model and improved fast and robust FCM algorithm for detection and classification of brain tumor from MR image

*Dr. Nagarjuna [1]*, Dr K Venkataramana[2]*

*[1]*Associate Professor,Dept. Of Computer Science and Engineering, NIT , BBSR*
*[2] Associate Professor,Dept. Of Computer Science and Engineering, NIT , BBSR*

*nagarjuna@thenalanda.com*, k.venkata@thenalanda.com*

**Abstract**
A novel modified adaptive sine cosine optimization algorithm (MASCA) integrated with particle swarm optimization (PSO) based local linear radial basis function neural network (LLRBFNN) model has been proposed for automatic brain tumor detection and classification. In the process of segmentation, the fuzzy C means algorithm based techniques drastically fails to remove noise from the magnetic resonance images. So, for reduction of noise and smoothening of brain tumor magnetic resonance image an improved fast and robust fuzzy c means algorithm segmentation algorithm has been proposed in this research work. The gray level co-occurrence matrix technique has been employed to extract features from brain tumor magnetic resonance images and the extracted features are fed as input to the proposed modified ASCA–PSO based LLRBFNN model for classification of benign and malignant tumors. In this research work the LLRBFNN model's weights are optimized by using proposed MASCA–PSO algorithm which provides a unique solution to get rid of the hectic task of radiologist from manual detection. The classification accuracy results obtained from sine cosine optimization algorithm, PSO and adaptive sine cosine optimization algorithm integrated with particle swarm optimization based LLRBFNN models are compared with the proposed MASCA–PSO based LLRBFNN model. It is observed that the result obtained from the proposed model shows better classification accuracy results as compared to the other LLRBFNN based models.

**Keywords** Fuzzy C means algorithm (FCM) · Fast and robust fuzzy C means algorithm (FRFCM) · Local linear radial basis function neural network (LLRBFNN) · Adaptive sine cosine optimization algorithm–particle swarm optimization (ASCA–PSO) · Sine cosine algorithm (SCA)

## 1 Introduction

In recent years, the death rate grows unanimously due the brain tumors at every age groups. According to the report published by the American Brain Tumor Association (ABTA) February 24, 2016 [1], that the children and young adults between 15 and 39 age group are affected due to malignant brain tumors. Between the age group 15–19 years olds, the cancer related deaths are growing rapidly as per the report. When the data is analysed in 5-year age incre- ments, the researchers found that the mentioned age groups are affected by different types of tumor which is not known at its early stage. Basically brain tumors are categorized as malignant and benign tumors, which grows abnormally in the brain. Malignant tumors contains cancerous cells which grows to all the parts of the brain due to non-uniform struc- ture. Benign tumors are of uniform structure and contains non-cancerous cells. When the brain tumor tissues grows slowly, it causes vision problem, vomiting tendency etc. to the patients. The complex structure of tumor diagnosis becomes a challenging task for the clinical doctors. In the study of biomedical imaging, magnetic resonance image plays a vital role of acquisition of brain tumors. Magnetic

✉

resonance imaging (MRI) with high resolution becomes most popular imaging techniques in the hospitals.

The manual diagnosis of the tumors by visualizing the magnetic resonance images in the clinic becomes a tedious and time-consuming task for doctors due to complex structure of the tumor and noise involvement in magnetic resonance (MR) imaging data. It is impossible to transform the image to a desired simpler condition by manual detection, which motivates us to propose a platform for automatic detection and classification of brain tumor from magnetic resonance image. So detection of tumor location and identification at earlier stage is essential to reduce the tumor related deaths. At the same time the classification of brain tumor is also essential to know the types of tumor present in the brain. By utilizing the segmentation and classification techniques, doctors can track and predict the uncontrollable growth of cancer affected areas at different levels to provide suitable diagnosis at early stage.

Segmentation of image from the magnetic resonance images is a consequential and arduous task for detection of brain tumor tissues. It becomes a challenging task due to the involute structure and variations in images. The different segmentation techniques such as FCM based genetic algorithm [2, 3], semi supervised learning with graph cuts [4], Berkele Wavelet transform [5, 6], Graphcut algorithm with co-segmentation for identification of exact cut point between edema and tumor [7], region growth segmentation [8], K-means clustering [9], spectral clustering [10, 11], wavelet transform image segmentation [12, 13], hidden markov random field models [14] etc. has been proposed for brain tumor segmentation. All mentioned segmentation algorithms aims to partitioning of data into clusters by minimizing the objective function and fails drastically remove noise from the magnetic resonance images. To improve the noise reduction capability and smoothening of magnetic resonance images, a novel improved FRFCM segmentation algorithm is proposed. The improved FRFCM technique is utilised to remove Rician noise from the magnetic resonance image in this research work.

Further, the classifiers such as support vector machine (SVM), probabilistic neural network (PNN), convolutional neural network (CNN) extreme learning machine (ELM) are some of the popular classifiers has already been used for classification of brain tumors. Due to the complex mathematical calculations and higher computational time requirements in the mentioned classifiers, we are motivated to propose a hybrid modified ASCA–PSO based LLRBFNN classification model for classification of brain tumors from magnetic resonance images. The proposed research work presents a novel image segmentation and classification technique for automatic detection and classification of brain tumor from magnetic resonance images.

The research work focuses on two contributions based on segmentation and classification. The contributions are summarised as follows:

- In first aspect, we are proposing an improvement to fast and robust FCM (FRFCM) based segmentation algorithm. The improvement has been made to the membership partition matrix of the FRFCM [15] algorithm and a wiener filter is employed to improve the Rician noise reduction capability. Further, the fuzzy membership value of the pixel has been updated to maintain image precision and smoothening of the magnetic resonance brain tumor images. The complete mathematical derivation has been developed for the new IFRFCM segmentation algorithm to maximize the segmentation accuracy.
- In the second aspect, we are proposing modifications to the parameters of hybrid adaptive sine cosine optimization integrated with particle swarm optimization (ASCA–PSO) [16] algorithm to maximize the optimization performance of the hybrid algorithm. The convergence parameter, position and velocity equations in the algorithm has been modified and the mathematical calculations with modification has been developed. Further, six bench mark functions are considered to validate the optimization performance of the proposed modified ASCA–PSO algorithm. With the modified convergence parameter, new velocity and position equations the proposed MASCA–PSO algorithm has been employed to optimize the weights of the LLRBFNN model for classification of brain tumor.

The paper is organized as follows. Section 2 presents the literature survey followed by research flow diagram, Sect. 3 presents the proposed improved fast and robust FCM segmentation technique, and Sect. 4 presents modified ASCA–PSO algorithm for LLRBFNN model, Sect. 5 presents the results and discussion and Sect. 6 presents conclusion and future scope followed by the reference.

## 2 Literature survey

In recent days researchers proposed image segmentation techniques based on FCM algorithms. Segmentation method is predicated on a rudimental region growing method and uses membership grades of pixels to relegate pixels into felicitous segments. From the literature survey, it is found that, FCM algorithm has ability to obtain texture and background information from the simple images, but failed in the case of complex noisy images where spatial information's are not considered. To overcome this problem, Ahmed et al. [17] proposed with spatial information (FCM_S) by considering intensity inhomogeneity, but the disadvantages is that

during computation the term spatial neighbour is considered in each epoch which takes more computational time. Further to reduce the computational burden, the spatial neighbourhood information has been proposed by Chen and Zhang [18] with spatial term. There are two variants FCM_S1 and FCM_S2 and both are not able to reduce Gaussian noise. Szilagyi et al. [19] proposed enhanced FCM algorithm (EnFCM) by using gray levels lesser value than the size of the image to reduce the time complexity burdens due to the spatial term. In EnFCM the parameter α (adjustable) plays a vital role for the improvement of segmentation results. To reduce noise and guarantee the detail-preservation of segmentation, the FGFCM (fast generalized FCM algorithm) has been proposed by Cai and Chen [20] with a similarity measure factor which improves the robustness of FCM, but FGFCM requires more parameters than the EnFCM. The fuzzy local information c-means clustering algorithm (FLICM), replaces the parameter α by a fuzzy factor in the objective function to delineate the noise and detail image preservation which is proposed by Krinidis and Chatzis [21]. For the development of a novel FCM algorithm, the algorithm should be free from selection of parameter. In this contrast FLICM, improves the segmentation process, but not free from parameter selection and also not perfect for local information of images and fails to remove Gaussian noise beyond 30%. To enhance the performance of FLICM Gong et al. [22] proposed kernel metric with local information for noise reduction which is free from selection of parameter. FCM with local information and kernel metric (KWFLICM) proposed by Gong et al. [23] to reduce noise and improve the robustness of FLICM. Guo et al. [24] proposed adaptive FCM algorithm based on noise detection (NDFCM), which is faster since the image filtering is done before starting of iterations. In this, the trade-off parameter has been tuned automatically by considering the local variance of image grey levels. To ameliorate the robustness to noise and avoid parameter, Tao Lei et al. [15] presented a fast and robust FCM (FRFCM), which is based on membership filtering and morphological reconstruction. FRFCM [15] uses median filtering to the membership partition matrix for noise reduction and improvement of segmentation accuracy. The local spatial information of images has been added into FRFCM by employing morphological reconstruction operation to guarantee noise level reduction and image detail-preservation. The FRFCM [15] employs more parameter, and fails to reduce Gaussian noise, salt and pepper noise and uniform noise from the synthetic image beyond 30%.

To improve the Rician noise removal capability of FRFCM algorithm, an improved fast and robust FCM algorithm (IFRFCM) has been proposed by improving the membership partition matrix and employing a wiener filter to the membership partition matrix of the FRFCM algorithm. The fuzzy membership value of the pixel has been updated to maintain image precision and smoothening of image. The proposed segmentation algorithm can provide good segmentation results for magnetic resonance images with high segmentation precision. We have taken eight previously proposed FCM based algorithms for the comparison with our proposed IFRFCM segmentation technique.

While considering for classification of brain tumors from magnetic resonance images, the classifiers such as support vector machine (SVM) with weighted kernel width achieves an accuracy of 89.92% for cancerous tumors proposed by Rezaei and Agahi [25]. Torheim et al. [26], uses texture features, SVM and achieved a classification accuracy of 87% for 3DMR images. Ruixuan Lang et al. [27] uses convolutional neural networks (CNNs) for 3D MR images and achieves the dice accuracy of 80%, Deepa et al. [28] proposed Extreme learning machine and genetic algorithm for classification of tumors and achieves 97.55% accuracy etc. The hybrid model PSO (Particle swarm optimization) based LLRBFNN Algorithm for automatic brain tumor detection proposed by Krishna [29]. There are different hybrid models such as LLRBFNN model with teaching learning based optimization (TLBO) weight optimization [30, 31] has been used for power signal classification, financial forecasting etc. Also the particle swarm optimization [32–35] technique which is based on bird flocking used in controller design, computational intelligence etc. Further the hybrid optimization algorithm PSO–GA (PSO–genetic algorithm) proposed by Garg [36] and de Fátima Araújoa and Uturbey [37] uses PSO–DE (PSO–differential evolution) for performance assessment to the dispatch of generation and demand, Dipankar Santra et al. [38] uses PSO–ACO (PSO–ant colony optimization) to solve economic load dispatch problem. It is observed from the literature survey that, there is not enough research work on automatic detection and classification of brain tumor utilizing hybrid biologically inspired hybrid optimized models. In this research work, we are proposing a modified ASCA–PSO hybrid algorithm to optimize the weights of LLRBFNN model. With the modification in ASCA–PSO algorithm, the performance of the classifier also increases.

The meta heuristic sine cosine algorithm (SCA) [39] has been hybridised with PSO by improvising the position equation of ASCA–PSO [16] algorithm. The sine cosine algorithm basically based on the trigonometric sine and cosine functions as operators for updation of the parameters [40, 41]. In ASCA–PSO hybrid algorithm, it is observed that still the parameters of the SCA algorithm needs proper tuning for maximizing the performance of optimization. In this research work, the learning parameter of ASCA–PSO hybrid algorithm has been modified by a inverse exponential factor which leads to new position and velocity equations which are utilized for optimization of weights of LLRBFNN classifier model. To validate the optimization performance of the proposed modified ASCA–PSO algorithm six bench

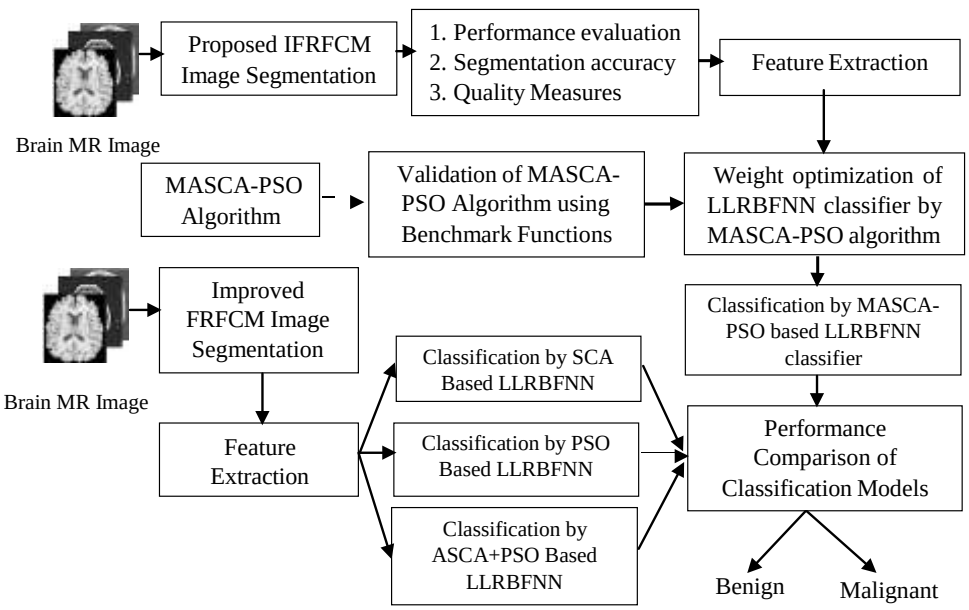


**Fig. 1** Block diagram of proposed methodology for classification of brain tumor from MRI

mark functions are considered for optimization and results are presented. After observation from the testing result performance, the proposed MASCA–PSO hybrid algorithm has been employed for weight optimization of LLRBFNN model.

### Block diagram of proposed methodology

The research work is focussing on the segmentation and classification of brain tumor from magnetic resonance image. The proposed methodology block diagram is presented in Fig. 1.

The research work follows the steps as (1) the brain MR images has been segmented by the improved fast and robust FCM (IFRFCM) algorithm at first step. After segmentation, the features has been extracted from the images using GLCM feature extraction technique. Further in the second step (2) the extracted features are fed as input to the PSO–LLRBFNN model, ASCA–PSO–LLRBFNN model and SCA–LLRBFNN model and proposed MASCA–PSO based LLRBFNN model, for the classification of brain tumors. In the third stage (3) and the weights of LLRBFNN model are updated utilizing MASCA–PSO algorithm and the classification comparison accuracy results from the classifiers are presented.

## 3 Proposed improved fast and robust FCM (IFRFCM) segmentation technique

The proposed improved fast and robust FCM segmentation improves noise reduction capability by employing a weiner filter to the modified membership partition matrix of the objective function of FCM algorithm with local information.

The objective function of the fuzzy c means algorithm with local information [21] is given by

$$J_s = \sum_{v=1}^{N}\sum_{k=1}^{c} u_{kv}^{m} \left\| x_v - v_k \right\|^2 + \sum_{v=1}^{N}\sum_{k=1}^{c} G_{kv} \tag{1}$$

where the fuzzy factor is given by

$$G_{kv} = \sum_{\substack{r \in N_v \\ v \neq r}} \frac{1}{d_{vr}+1} \left(1 - u_{kr}^{m}\right) \left\| x_r - v_k \right\|^2 \tag{2}$$

where the spatial Euclidean distance between pixels $x_v$ and $x_r$ is denoted by $d_{vr}$ , $N_v$ is the set of neighbours within a window around $x_v$ and $x_r$ represents the neighbours of $x_v$ and $u_{kr}$ is the neighbours of $u_{kv}$. With respect to cluster $k$ , $x_v$ is the gray value of the $k$th pixel, $u_{kv}$ represents the fuzzy membership value of the $v$th pixel and $N$ is the total number of pixels in the gray scale image $f = [x_1, x_2, \cdots, x_N]$, $x_v$ is the gray value of $v$th pixel, denotes the cluster centre and determines the fuzziness of the consequential partition.

With the fuzzy factor $G_{kv}$, the capability of noise reduction improves. The fuzzy partition matrix is given by

$$u_{kv} = \frac{1}{\sum_{j=1}^{c} \left( \frac{\left\| x_v - v_k \right\|^2 + G_{kv}}{\left\| x_v - v_j \right\|^2 + G_{jv}} \right)^{\frac{1}{m-1}}} \tag{3}$$

and

$$v_k = \frac{\sum_{k=1}^{N} u^{m}_{kv} x_v}{\sum_{v=1}^{N} u_{kv}} \tag{4}$$

From Eq. (3), it is found that the factor $G_{kv}$ is completely free of using any parameter that controls the balance between the image noise and the image details, but computational complexity increases. Clearly, there is a contradiction between improving the robustness and reducing the computational complexity simultaneously for FCM.

To reduce the computational complexity, the membership partition matrix is modified as

$$G_{kv}^{f} = \sum_{\substack{r \in N_v \\ v \neq r}} \frac{\log(\zeta^{r})}{\exp(d_{vr}) + 1} u_{kr}^{m} \| x_r - v_k \|^2 \tag{5}$$

where $u_{kr}$ is the neighbours of $u_{kv}$, $\zeta$ is gray value of image and is the smoothness parameter between 0 and 1. Further, considering the morphological reconstruction operations such as dilation and erosion, the reconstruction of the image is considered as $\zeta_p$, which is given by

$$\zeta_p = R_e^C(f) \tag{6}$$

where $R^C$ represents the morphological closing reconstruction which is efficient for noise removal and $f$ denotes an original image and reconstruction operators considering morphological closing reconstruction is given by

$$R^C(f) = R^{\beta}_{R_f^{\beta}(\beta(f))}(\beta(f)) \tag{7}$$

where $\beta$ is the erosion operation, $\beta$ is the dilation operation, is the closing operation and $f$ represents original image. With image reconstruction operation, the filtering capability increases. Now, with morphological closing reconstruction the objective function is modified as

$$J_s = \sum_{k=1}^{c} \sum_{p=1}^{q} u_{kp}^{m} \| \zeta_p - v_k \|^2 + \sum_{k=1}^{c} \sum_{p=1}^{q} G_{kp} \tag{8}$$

From Eq. (8), it is evident that $u_{kp}$ represents the degree of membership of gray value $p$ in cluster $k$, $\zeta_p$ is a gray level, $1 \le p \le q$, $q$ represents the gray levels contained in $\zeta$. Then the modified fuzzy factor is given by

$$G_{kp}^{f} = \sum_{\substack{r \in q_v \\ v \neq r}} \frac{\log(\zeta^{r})}{\exp(d_{vr}) + 1} u_{kp}^{m} \| \zeta_p - v_k \|^2 \tag{9}$$

where

$$u_{kp} = \frac{1}{\sum_{j=1}^{\left( \frac{\| \zeta_p - v_k \|^2 + G_{kp}^{f}}{\| \zeta_p - v_j \|^2 + G_{jp}^{f}} \right)^{\frac{1}{m-1}}}} \tag{10}$$

and

$$v_k = \frac{\sum_{k=1}^{c} u_{kp}^{m} \zeta_p}{\sum_{p=1}^{q} u_{kp}} \tag{11}$$

Now, we can write the membership partition matrix in the form as $U = u_{kp}^{c \times q}$. Further, Considering convergence speed of the algorithms and the performance of the partition matrix $U$ we employ a wiener filter [3, 42]. The new membership partition matrix is given by

$$U^{l} = wiener[U] \tag{12}$$

The steps of implementation of the algorithm is as follows:

*Step 1* Choose the cluster value , filtering window size , and fuzzification coefficient , maximum number of iteration at the beginning.
*Step 2* Set loop counter $l = 0$ and update the cluster centre using Eq. (11).
*Step 3* Initialize the membership partition matrix randomly
*Step 4* By using the equation $\zeta_p = R_e^C(f)$, compute the new image.
*Step 5* Update $U^l$ according to Eq. (12) until convergence of objective function, else go to step 2.

## 4 Modified adaptive sine cosine optimization algorithm integrated with particle swarm optimization (MASCA–PSO) algorithm

Due the complexity involved in learning parameter, the position equation and velocity equation of the ASCA–PSO took more computational time for convergence. The modification in the learning parameter leads to new velocity and position equation. The mathematical calculations are presented for the hybrid modified ASCA–PSO (MASCA–PSO) to maximize the performance of the optimization. To validate the performance of the proposed MASCA–PSO algorithm six bench mark functions are considered. The PSO [32–35] algorithm the velocity and position equations are as follows.

The velocity update equation is given by

$$v_i(n+1) = z \times v_i(n) + \beta_1 r_1 \left( p_i^{best} - x_i(n) \right) + \beta_2 r_2 \left( p^{gbest} - x_i(n) \right) \tag{13}$$

And the position update equation is given by

$$x_i(n+1) = x_i(n) + v_i(n+1) \tag{14}$$

where is inertia coefficient, the Learning factors $\beta_1$ represents the local position weight coefficient and $\beta_2$ represents the global position weight coefficient.

According to sine cosine algorithm the position equation is updated as

$$X_i^{n+1} = \begin{cases} X_i^n + \alpha_1 \times \sin(\alpha_2) \times \left| \alpha_3 p_{gbest}^j - X_i^j \right|, & \alpha_4 < 0.5 \\ X_i^n + \alpha_1 \times \cos(\alpha_2) \times \left| \alpha_3 p_i^j - X_i^j \right|, & \alpha_4 \geq 0.5 \end{cases} \quad (15)$$

where $\alpha_1$, $\alpha_2$, $\alpha_3$, $\alpha_4$ are the random variables and $\alpha_1$ is given by

$$\alpha_1 = a\left(1 - \frac{n}{K}\right) \quad (16)$$

where is the current iteration, K is the maximum number of iterations.

The $X_i^n$ represents the current position and $X_i^{n+1}$ represents the update position. Here $|\cdot|$ represents the absolute value. The parameter $\alpha_1$ determines the next position regions of the search and explores to search the space to a higher value. The parameter $\alpha_2$ represents the direction of movement of towards or away from $x_i(n)$. The parameter $\alpha_3$ controls the current movement, during each iteration $\alpha_1$, $\alpha_2$, $\alpha_3$ are updated and the parameter $\alpha_4$ equally switches between the sine and cosine functions.

For fast convergence of the parameter $\alpha_1$ is modified as

$$\alpha_{11} = \frac{1}{1 + \exp(\alpha_1)} \quad (17)$$

And the corresponding position equation is given with modification factor presented as

$$X_{ij}^{n+1} = \begin{cases} X_{ij}^n + \alpha_{11} \times \sin(\alpha_2) \times \left| \alpha_3 y_i^n - X_i^j \right|, & \alpha_4 < 0.5 \\ X_{ij}^n + \alpha_{11} \times \cos(\alpha_2) \times \left| \alpha_3 y_i^n - X_i^j \right|, & \alpha_4 \geq 0.5 \end{cases} \quad (18)$$

The PSO parameters update their positions and obtains the best solution $y_g^{gbest}$. The velocity and position update equation is given by

$$v_i(n+1) = z \times v_i(n) + \beta_1 r_1 \left( y_{best_i} - x_i(n) \right) + \beta_2 r_2 \left( y_g^{gbest} - x_i(n) \right) \quad (19)$$

$$y_i(n+1) = y_i^n(n) + v_i^n(n+1) \quad (20)$$

The $x_{ij}$ is influenced by the best solutions of the group in the PSO layer $y_i$ and $y_i$ is influenced by the best solution between the whole set of individuals in the $y_g^{gbest}$. To validate the optimization performance of the modified ASCA–PSO hybrid algorithm six benchmark functions [43, 44] are presented in Table 4, and the corresponding comparison optimization results are shown in Fig. 4a–f in Sect. 5.2.

### 4.1 Proposed modified ASCA–PSO weight optimization LLRBFNN model

The automatic classification of tumor tissues has been carried out by the proposed hybrid MASCA–PSO based LLRBFNN model. The weights of the LLRBFNN (local linear radial basis function neural network) model has been optimized by hybrid MASCA–PSO algorithm. Also the position equation of the ASCA–PSO algorithm and SCA parameter has been improved to get the faster weight optimization of the LLRFNN model which leads to unique classification of brain tumor tissues. The proposed MASCA–PSO based LLRBFNN model is presented in this section for classification. The weights are updated by APSO algorithm.

The motivation to use LLRBFNN [29, 30] model for this research work is that the weights of the model replaces a local linear model between output layer and the hidden layer of RBFNN which reduces the overall nodes requirement in the network. This model also provides better result to the pattern classification task than the multilayer perceptron (MLP), PNN (probability neural network) and RBFNN. The weights of the LLRBFNN Model is optimised with PSO, SCA, ASCA–PSO and MASCA–PSO algorithm and the results were compared.

The input $X = [x_1, x_2, \cdots, x_n]$ are the feature data points taken as inputs to the LLRBFNN model shown in Fig. 2 and $Z_1$, $Z_2$, …, $Z_N$ are radial Gaussian activation function in the hidden units.

The hidden activation function is given by

$$Z_n(x) = e^{\frac{-\|x - c_n(n)\|^2}{2\sigma_n^2}} \quad (21)$$

where $\sigma_n^2$ represents the controlling parameter, $c_N$ represents the centre and the Euclidean distances given by $\|x - c_i(n)\|$.

Mean square error is obtained by minimizing the objective function as

$$MSE(e) = \frac{1}{N} \sum_{n=1}^{N} \left( d_n - y_n \right)^2 \quad (22)$$

where "d" is the desired vector.

In this network the weights are initialized to zero and optimized by using MASCA–PSO algorithm. The parameters taken in this work as Maximum velocity = 1.0, minimum velocity $= -1.0$, $a = 2$, $\beta_1 = 0.5$, $\beta_2 = 0.5$. The population size is taken as 100 and the maximum number of 1000 iterations are considered for execution.

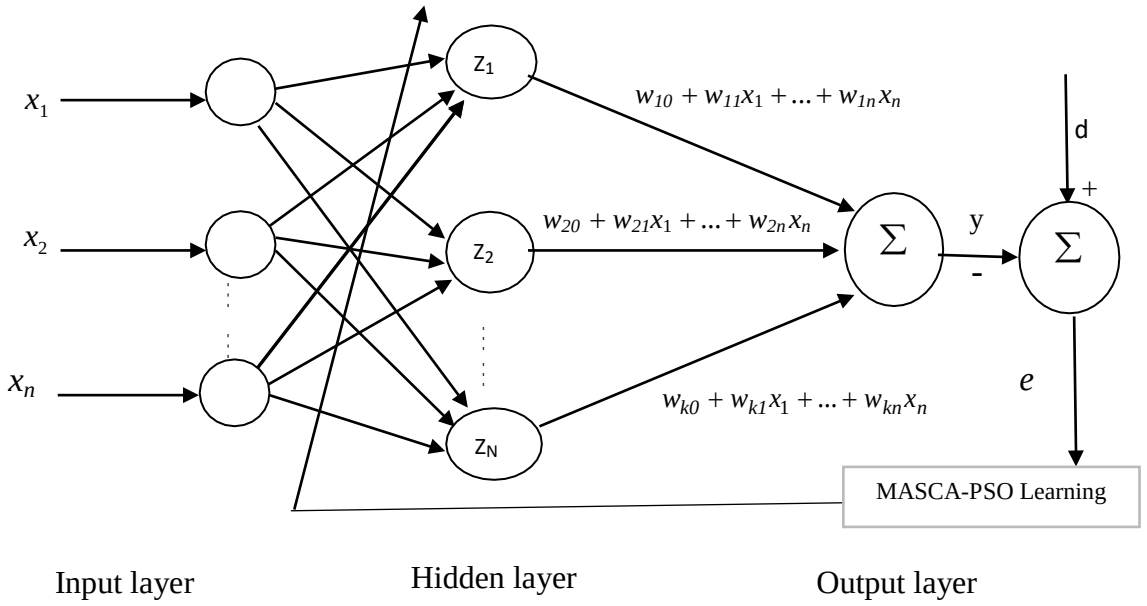


**Fig. 2** MASCA–PSO based LLRBFNN

**MASCA-PSO Algorithm implementation for weight optimization of LLRBFNN Model.**

1. Initializing particles (weights) with random position and velocity vectors.
2. Initialize the MASCA parameters $\alpha_{11}, \alpha_2, \alpha_1, \alpha_4$ and PSO parameters $\chi, \beta_1, \beta_2$
3. Evaluate the objective function in the next phase to evaluate fitness based on $x_{ij}$
4. Update $y_i$ and $y_g^{best}$ for best fit
5. %Program loop
6. for i=1:L
7. for j=1:N
8. update( $x_{ij}$ )
9. if $(x_{ij} < y_i)$ *then* $y_i = x_{ij}$
10. update SCA parameter
11. update $y_i$ and $y_g^{gbest}$
12. end for the loop j
13. Continue until (K< maximum number of iteration)
14. Stopping criteria: getting $y_g^{best}$ as optimal solution
15. If not converges, Go to step 6, and repeat until convergence is satisfied.

The weights of the LLRBFNN classifier has been optimized with proposed MASCA–PSO algorithm. The extracted features are fed as input to the modified ASCA + PSO based LLRBFNN model which is shown in Fig. 4 for classification. Further the weights of LLRBFNN model are optimized with PSO, SCA, ASCA–PSO and accuracy results are presented in Table 13.

## 5 Result and discussion

### Segmentation results utilizing proposed Improved FRFCM algorithm

We have considered the magnetic resonance image of size 256 × 256 corrupted by Rician noise [45, 46] with $\sigma_n$ = 10 and $\sigma_n$ = 20, and the results has been presented in Fig. 2a–k. The magnetic resonance image of Alzheimer's disease is

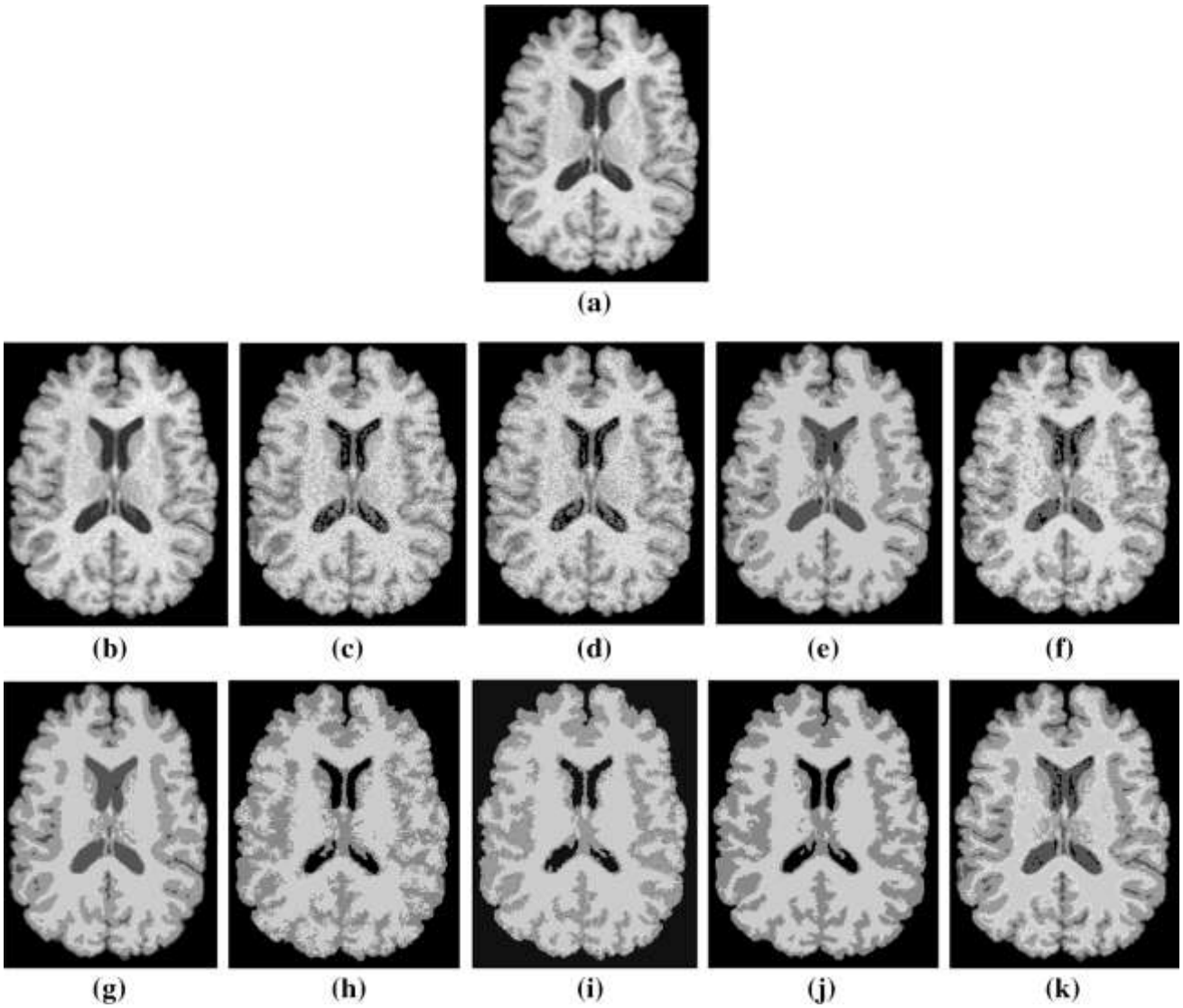


**Fig. 3** Segmentation results on the MR image corrupted by Rician noise ($l=9$). **a** Original image. **b** Image corrupted by Rician noise. **c** FCM result. **d** FCM_S1 result. **e** FCM_S2 result. **f** EnFCM result. **g** FLICM result. **h** KWFLICM result. **i** NDFCM result. **j** FRFCM result. **k** IFRFCM result

taken from brain database [47, 48] for the purpose of segmentation.

Figure 3c–k shows segmentation results of proposed IFRFCM algorithm and all other mentioned algorithms. Due to the mean filter, The FCM S1 obtains a poor segmentation, but FCM S2 obtains a somehow better segmentation result than FCM and FCM S1 as the median filters employed by FCM S2. It can be seen that from the segmentation results that the performance of EnFCM, FCM S1, FCM S2 are not up to the mark, while KWFLICM, NDFCM FRFCM and IFRFCM shows satisfactory results of denoising. It is observed that the proposed IFRFCM algorithm shows better visual denoising result than the other algorithms. The proposed IFRFCM utilizes a modified partition matrix which gives proximately kindred result in terms performance evaluation, but has good visual effect than the other algorithms.

## Segmentation performance evaluation

The performance result of segmentation is evaluated by segmentation accuracy (SA), and a quantitative index score (S) [19]. The segment accuracy is given by

$$SA = \frac{\sum_{k=1}^{c} A_k \cap C_k}{\sum_{j=1}^{c} C_j} \quad (23)$$

and

**Table 1** Segmentation performance evaluation

| Image | Time in seconds | | | | | | | | |
|---|---|---|---|---|---|---|---|---|---|
| | FCM | FCM S1 | FCM S2 | EnFCM | KWFLICM | FLICM | NDFCM | FRFCM | IFRFCM |
| Img-1 | 3.85 | 2.28 | 2.23 | 1.98 | 9.34 | 16.04 | 4.66 | **1.52** | **0.36** |
| Img-2 | 4.15 | 2.29 | 2.16 | 2.15 | 9.27 | 18.63 | 3.8 | 1.32 | 0.33 |
| Img-3 | 4.69 | 2.19 | 2.1 | 2.15 | **9.31** | 11.49 | **4.06** | **1.36** | **0.31** |
| Img-4 | 3.48 | 2.2 | 2.21 | 2.39 | 9.12 | 10.07 | 2.88 | 0.44 | 0.25 |
| Img-5 | 3.28 | 2.11 | 2.34 | 1.15 | **8.87** | 9.89 | **3.23** | **0.54** | **0.24** |
| Img-6 | 3.45 | 3.23 | 2.35 | 1.62 | 8.45 | 10.34 | 2.34 | 0.46 | 0.35 |
| Img-7 | 4.35 | 3.11 | 3.03 | 1.22 | 9.34 | 11.12 | 2.35 | 0.45 | 0.37 |
| Img-8 | 4.22 | 3.12 | 3.11 | 1.66 | 9.46 | 11.22 | 2.21 | 0.54 | 0.33 |
| Img-9 | 3.96 | 3.67 | 3.27 | 1.64 | 9.89 | 12.92 | 2.11 | 0.34 | 0.29 |
| Img-10 | 3.98 | 3.49 | 3.21 | 1.45 | 10.12 | 11.32 | 2.45 | 0.52 | 0.32 |

Bold values represents the segmentation performance

**Table 2** Segmentation accuracy

| Algorithm | Noise level | |
|---|---|---|
| | Rician noise ($\sigma_n$ = 10) | Rician noise ($\sigma_n$ = 20) |
| FCM | 91.28 | 88.12 |
| FCM S1 | 96.85 | 90.34 |
| FCM S2 | 98.81 | 95.62 |
| En FCM | 98.72 | 96.84 |
| FLIFCM | 98.65 | 96.27 |
| KWFLICM | 98.82 | 97.01 |
| NDFCM | 99.92 | 98.61 |
| FRFCM | **99.95** | **99.12** |
| IFRFCM | **99.96** | **99.36** |

Bold values represents the best result obtained in terms of segment accuracy

$$S = \frac{\sum_{k=1}^{c} A_k \cap C_k}{A_k \cup C_k} \quad (24)$$

where $c$ represents number of the cluster and $A_k$ represents the set of pixels which belongs to the $k$th class while $C_k$ is the set of pixels in the Ground Truth. Tables 1 and 2 presents the computational time of the nine algorithms including IFRFCM algorithm and the segmentation accuracy in percentage. The proposed improved FRFCM segmentation technique provides noise free magnetic resonance images for tumor detection. The performance analysis of segmented images were calculated and presented in the Table 1. The segmentation accuracy by the proposed IFRFCM is better than the other FCM based algorithm is shown in Table 2. In some cases both the segmentation processes FRFCM and IFRFCM shown the nearly similar results, still the proposed IFRFCM segmentation is preferred due to robust capability of reduction of Rician noise.

## Quality measures

To compare the performance of the different algorithms, two quality indexes are considered as structural similarity (SSIM) index and the quality index based on local variance (QILV) [49, 50]. Both quality indexes provides structural similarity between the ground truth and the estimated images. However, SSIM is more sensitive to the noise level

**Table 3** Quality measures for the MR image with Rician noise

| Algorithm | Rician noise | | | | | |
|---|---|---|---|---|---|---|
| | $\sigma_n$ = 10 | | | $\sigma_n$ = 20 | | |
| | SSIM | QILV | PSNR (dB) | SSIM | QILV | PSNR (dB) |
| FCM | 0.7621 | 0.6856 | 18.23 | 0.6912 | 0.6432 | 16.11 |
| FCM S1 | 0.7834 | 0.7178 | 18.67 | 0.7146 | 0.6745 | 16.87 |
| FCM S2 | 0.7889 | 0.7624 | 19.56 | 0.7722 | 0.7278 | 17.12 |
| En FCM | 0.7982 | 0.8346 | 20.02 | 0.7813 | 0.8123 | 19.87 |
| FLIFCM | 0.8349 | 0.9098 | 26.78 | 0.8182 | 0.8672 | 23.14 |
| KWFLICM | 0.8467 | 0.9147 | 28.12 | 0.8287 | 0.8712 | 25.83 |
| NDFCM | 0.8731 | 0.9262 | 29.47 | 0.8542 | 0.8892 | 27.41 |
| FRFCM | **0.9176** | **0.9478** | **33.78** | **0.8739** | **0.9214** | **31.31** |
| IFRFCM | **0.9318** | 0.9887 | **38.45** | **0.9129** | 0.9543 | **36.29** |

Bold values represents the quality measure in terms of rician noise model

in the image and the QILV to blurring of the edges. In addition to the both, the PSNR (peak signal to noise ratio) is also calculated. Table 3 shows the experimental results for two different values of $\sigma_n = 10$ and $\sigma_n = 20$. It is also observed that when $\sigma_n = 10$, the quality measure PSNR value is 38.45 dB and 33.78 dB in case of proposed IFRFCM and FRFCM segmentation techniques respectively. The higher value of PSNR in case of IFRFCM indicate better signal-to noise ratio in the extracted image. Also the larger value of SSIM indicates the noise reduction in the extracted image which is presented in Table 3.

When compared with the proposed Improved FRFCM technique with other techniques with Rician noise model, the IFRFCM show a better performance in terms of noise reduction which indicates a larger value of SSIM and the image edges are preserved as per the increased value of QILV of the proposed IFRFCM algorithm. The noise reduction performance of the NDFCM and FRFCM are good, but, as per the QILV value, it shows image blurring which leads to loss of image information at the border and the image edges.

## Performance validation of proposed MASCA–PSO

The experiments are carried out with Matlab 2017a software, CPU core I5 with 4 GB RAM. For the experiment the population size of 100 and number of iteration are taken as 1000. SCA algorithm has the high searching computational capability, but the next position change is based on random and adaptive variable which gives unsatisfactory solutions. The lack of internal memory SCA will not be able to keep track of previous solutions. During the process of optimization SCA rejects all fitness values and never preserves the possible set of solutions. Due to this it starts converging slowly and may stuck at local minima. To overcome the difficulties faced by SCA, the particle swarm optimization (PSO) algorithm has been integrated with sine cosine algorithm, in which PSO provides internal memory to SCA to keep track of all possible solutions to converge to global optima [51]. Six benchmark functions [43, 44] were considered to justify the optimization capability of proposed

**Table 5** Parameters and values of optimization algorithm

| Algorithm | Parameter | Value |
|---|---|---|
| SCA | | 2.0 |
| | $_1$ | 1.0 |
| | $_2$ | Random (0, 2$\pi$) |
| | $_3$ | 0.5 |
| PSO | Maximum velocity ($V_{max}$) | 1.0 |
| | Minimum velocity ($V_{min}$) | −1.0 |
| | $\beta_1$ (cognitive coefficient) | 0.5 |
| | $\beta_2$ (cognitive coefficient) | 0.5 |
| SSA | $C_1$ (cognitive coefficient) | 100 |
| | $C_2$, $C_3$ | Random (0, 1) |
| WAO | $\overline{a}$ (linearly decreased vector from 2 to zero) | 2 |
| | $\overline{r}$ | 2 |
| GWO | $\overline{a}$ (linearly decreased vector) | 2 |
| | $r1$, $r2$ (random vectors) | (−1, 1) |
| MFO | $b$ (for defining the shape of the logarithmic spiral constant) | 1.0 |
| | $t$ (random number) | (−1, 1) |
| ABC | The maximum cycle number | 100 |
| | Modification rate | 0.8 |
| ASCA–PSO | a | 2.0 |
| | $\alpha_1$ | 1.0 |
| | $\alpha_2$ | 0.5 |
| | $\alpha_3$ | 1.5 |
| | $\beta_1$, $\beta_2$ | 0.5 |

**Table 4** Benchmark functions for testing the proposed MASCA–PSO algorithm

| Function | Name of the function | Details | Dimension | Bound regions |
|---|---|---|---|---|
| F1 | Ackley's function | $-20\,e^{-0.2\sqrt{\frac{1}{d}\sum_{i=1}^{d} x_i^2}} - e^{\frac{1}{d}\sum_{i=1}^{d}\cos(2\pi x_i)} + 20 + e^1$ | 30 | (−32, 32) |
| F2 | Rastrigin function | $10d + \sum_{i=1}^{d}\left(x_i^2 - 10\cos(2\pi x_i)\right)$ | 30 | (−5.12, 5.12) |
| F3 | Griewanks's function | $\sum_{i=1}^{d}\frac{x_i^2}{4000} - \prod_{i=1}^{d}\cos\left(\frac{x_i}{\sqrt{i}}\right) + 1$ | 30 | (−600, 600) |
| F4 | Quartic Function | $\sum_{i=1}^{d} i x_i^4$ | 30 | (−1.28, 1.28) |
| F5 | Sphere function | $\sum_{i=1}^{d} x_i^2$ | 30 | (−5.12, 5.12) |
| F6 | Step 2 function | $\sum_{i=1}^{d} \lfloor x_i + 0.5 \rfloor^2$ | 30 | (−100, 100) |

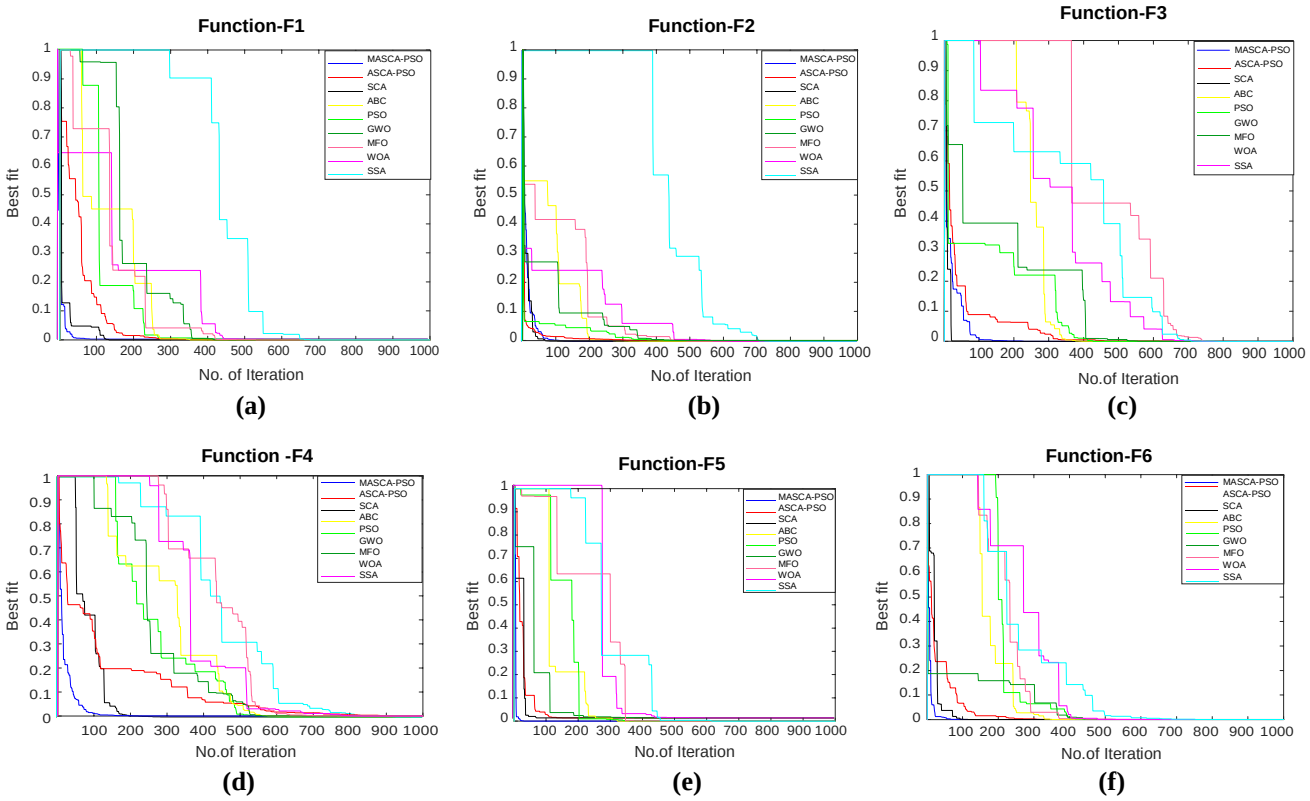


**Fig. 4** **a–f** Fitness curve of all algorithms

**Table 6** Computational time taken by all algorithm for functions F1–F6

| FUNCTION | ABC | PSO | GWO | MFO | WOA | SSA | SCA | ASCA–PSO | MASCA–PSO |
|---|---|---|---|---|---|---|---|---|---|
| F1 | 3.24 | 3.53 | 6.72 | 7.05 | 8.63 | 17.41 | **1.91** | **3.05** | **1.89** |
| F2 | 3.37 | 2.30 | 6.75 | 4.52 | 6.05 | 17.38 | **1.71** | **2.11** | **1.81** |
| F3 | 4.21 | 3.61 | 6.77 | 6.54 | 7.85 | 17.44 | 1.92 | 3.09 | 1.98 |
| F4 | 1.85 | 3.30 | 6.82 | 6.34 | 7.80 | 17.33 | 1.81 | **3.07** | **1.81** |
| F5 | 1.62 | 2.02 | 6.72 | 5.71 | 7.72 | 17.60 | **1.49** | 1.85 | **1.52** |
| F6 | 2.37 | 1.95 | 6.81 | 5.54 | 7.52 | 19.33 | 1.51 | 1.88 | 1.35 |

Bold values represents the best result obtained in terms of computation time

MASCA–PSO algorithm which is shown in the Table 4. The parameters and values used during evaluation of optimization is presented in Table 5.

To justify the performance of the proposed modified ASCA–PSO (MASCA–PSO) algorithm, six benchmark functions were tested with PSO [32], ASCA–PSO [16], SCA [39], slap swarm algorithm (SSA) [52], grey wolf optimization (GWO) [53], whale optimization algorithm (WOA) [54], moth flame optimization (MFO) [55], artificial bee algorithm (ABC) [56, 57] along with the proposed MASCA–PSO algorithm. The results of all the algorithm presented from Fig. 4a–f.

It can be seen from the Fig. 4a–f that the proposed MASCA–PSO algorithm took less time to converge in all the six functions in comparison to the mentioned algorithms. The function F1–F6 are all tested by all nine algorithms which are shown from Fig. 4a–f. The computational time taken by algorithms for six functions is presented in the Table 6.

It is evident from the above table that the computational time taken by the proposed MASCA–PSO algorithm is nearly same to the SCA (sine cosine algorithm) algorithm, but the proposed algorithm is free from local minima.

## 6 Database

In this research work, we have considered Dataset-160 and Data-255 from Harvard medical school of architecture (http://med.harvard.edu/AANLIB/) [47]. For our

**Table 7** Dataset details

| Dataset | Total number of images | | Images for training | | Images for testing | |
|---|---|---|---|---|---|---|
| | Normal | Abnormal | Normal | Abnormal | Normal | Abnormal |
| Dataset-160 | 20 | 140 | 16 | 112 | 4 | 28 |
| Dataset-255 | 35 | 220 | 28 | 176 | 7 | 44 |

**Table 8** Extracted values of the feature for Dataset-255

| Sl. no. | Features | Values |
|---|---|---|
| 1 | Correlation | 0.2316 |
| 2 | DM | 0.8183 |
| 3 | Entropy | 2.1834 |
| 4 | Coarseness | 2.2354 |
| 5 | Homogeneity | 0.9346 |
| 6 | Kurtosis | 0.3114 |
| 7 | Energy | 0.1547 |

experiment, we have considered Dataset-160 which consists of (Normal-20, Abnormal-140) and Dataset-255, consists of 255 (35 normal and 220 abnormal) T2-weighted magnetic resonance 256 × 256 axial plane brain images (Table 7). Abnormal brain MR images of Dataset-255 are from 11 types of diseases, among which 7 types of diseases are same as the Dataset-160. Dataset-160 contains seven types of diseases [58, 59] such as Huntington's disease, Alzheimer's disease, Alzheimer's disease plus visual agnosia, glioma, meningioma, Pick's disease, sarcoma. The Dataset-255 consists abnormal images of 4 new types of diseases: chronic subdural hematoma, cerebral toxoplasmosis, herpes encephalitis and multiple sclerosis.

### Feature extraction

The statistical textural features such as correlation, DM (directional moment), entropy, coarseness, kurtosis, homogeneity and energy were extracted using gray-level co-occurrence matrix (GLCM) [60, 61] technique for classification. The statistical textural feature values presented in the Table 8. These extracted features were used as input vectors for training and testing the performance of MASCA–PSO based LLRBFNN classifier.

## 6.2 Performance measure of classifiers

For our experiment, we have considered Dataset-160 and Dataset-255 having T2-weighted magnetic resonance brain images. We have used 5 × 5 cross validation procedure to avoid over fitting problem. Sensitivity, specificity, accuracy are the measure of system performance in classification of normal and abnormal brain tumor MR images [58]. Sensitivity shows the true positive rate in identifying the brain tumor, which calculates correctly classified number of abnormal images out of total number of abnormal brain MR images. Specificity shows the true negative rate in identifying the condition of normal brain, which calculates the number of normal brain MR images correctly classified out of the total number of normal MR images. The accuracy is the measurement of system effectiveness in conducting the whole classification, which calculates the total number of brain MR images that are correctly classified itself. The terms [58] utilized for performance measure evaluations are as follows:

TP = number of abnormal images correctly classified
TN = number of normal images correctly classified
FP = number of normal images classified as abnormal
FN = number of abnormal images classified as normal

$$Sensitivity = \frac{TP}{TP+FN}$$

$$Specificity = \frac{TN}{TN+FP}$$

$$Accuracy = \frac{TP+TN}{TP+TN+FP+FN}.$$

The 5 × 5-fold cross validation procedure calculations during each run of Dataset-160 and Dataset-255 are presented

**Table 9** 5 × 5-Fold cross validation procedure for **Dataset-160** during each run (MASCA–PSO)

| | Fold-1 | Fold-2 | Fold-3 | Fold-4 | Fold-5 | Total | Accuracy (%) |
|---|---|---|---|---|---|---|---|
| Run-1 | 32 | 31 | 32 | 32 | 32 | 159 | **99.375** |
| Run-2 | 32 | 32 | 32 | 32 | 32 | 160 | 100 |
| Run-3 | 32 | 32 | 32 | 32 | 31 | 159 | 99.375 |
| Run-4 | 32 | 32 | 32 | 32 | 32 | 160 | 100 |
| Run-5 | 32 | 32 | 32 | 32 | 32 | 160 | 100 |
| Final result | | | | | | | **99.875** |

Bold values represents the accuracy for Datase-160

Accuracy in percentage = (99.375 + 100 + 100 + 100 + 100)/5 = 99.875

**Table 10** 5 × 5-Fold cross validation procedure of Run-1 for **Dataset-160** of (MASCA–PSO)

| Fold | Test instances | TP | FN | TN | FP | Accuracy (%) |
|---|---|---|---|---|---|---|
| Fold-1 | 32 | 28 | 0 | 4 | 0 | 100 |
| Fold-2 | 32 | 27 | 1 | 4 | 0 | 96.875 |
| Fold-3 | 32 | 28 | 0 | 4 | 0 | 100 |
| Fold-4 | 32 | 28 | 0 | 4 | 0 | 100 |
| Fold-5 | 32 | 28 | 0 | 4 | 0 | 100 |
| Final result | | | | | | **99.375** |

Bold values indicates the confirmation of fold wise first run calculations accuracy with Table-9 for Dataset-160

First run accuracy in percentage = (100 + 100 + 96.875 + 100 + 100)/5 = 99.375

**Table 11** 5 × 5-Fold cross validation procedure for **Dataset-255** during each run (MASCA–PSO)

| | Fold-1 | Fold-2 | Fold-3 | Fold-4 | Fold-5 | Total | Accuracy (%) |
|---|---|---|---|---|---|---|---|
| Run-1 | 51 | 51 | 50 | 51 | 50 | 253 | **99.2156** |
| Run-2 | 51 | 51 | 51 | 51 | 51 | 255 | 100 |
| Run-3 | 51 | 50 | 50 | 51 | 50 | 252 | 98.82 |
| Run-4 | 51 | 51 | 51 | 51 | 51 | 255 | 100 |
| Run-5 | 51 | 51 | 51 | 51 | 51 | 255 | 100 |
| Final result | | | | | | | **99.61** |

Bold values indicates the accuracy for Dataset-255

**Table 12** 5 × 5-Fold cross validation procedure of Run-1 for **Dataset-255** of (MASCA–PSO)

| Fold | Test instances | TP | FN | TN | FP | Accuracy (%) |
|---|---|---|---|---|---|---|
| Fold-1 | 51 | 44 | 0 | 7 | 0 | 100 |
| Fold-2 | 51 | 44 | 0 | 7 | 0 | 100 |
| Fold-3 | 51 | 43 | 1 | 7 | 0 | 98.039 |
| Fold-4 | 51 | 44 | 0 | 7 | 0 | 100 |
| Fold-5 | 51 | 43 | 1 | 7 | 0 | 98.039 |
| Final result | | | | | | **99.2156** |

Bold values indicates the confirmation of fold wise first run calculations accuracy with Table-11 for Dataset-255

**Table 13** Performance measure of different classifiers

| Classifier | Dataset-160 | | | Dataset-255 | | |
|---|---|---|---|---|---|---|
| | Sensitivity | Specificity | Accuracy in (%) | Sensitivity | Specificity | Accuracy in (%) |
| PSO + LLRBFNN | 0.97 | 0.85 | 95.50 | 0.98 | 0.94 | 97.96 |
| SCA + LLRBFNN | 0.99 | 0.90 | 97.76 | 0.97 | 1.0 | 98.35 |
| ASCA + PSO + LLRBFNN | 0.98 | 1.0 | 98.75 | 0.99 | 0.94 | 98.97 |
| MASCA + PSO + LLRBFNN | 0.99 | 1.0 | **99.875** | 0.99 | 1.0 | **99.61** |

Bold values indicates the accuracy of different classification techniques

in Tables 9 and 11. Tables 10 and 12 shows the 5 × 5-fold cross validation procedure for first run of Dataset-160 and Dataset-255. The calculations are considered for modified ASCA–PSO based LLRBFNN classifier.

It is found that the proposed modif ied ASCA + PSO + LLRBFNN is better than other classifiers in terms of sensitivity, specificity and accuracy. Table 13 shows the performance measure of all classifiers for Dataset-160 and Dataset-255. The fivefold cross validation procedure have been employed for all the algorithms using Dataset-160 and Dataset-255. The accuracy obtained for Dataset-160 with PSO + LLRBFNN, SCA + LLRBFNN, ASCA + PSO + LLRBFNN, MASCA + PSO + LLRBFNN are 95.50%, 97.76%, 98.75%, 99.875% respectively. The

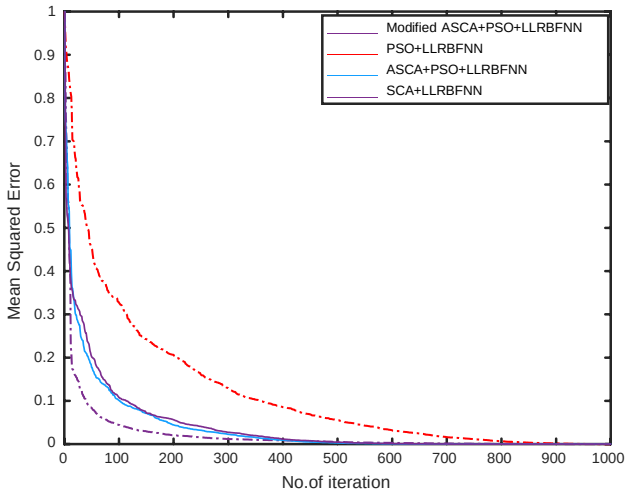


**Fig. 5** Mean squared error convergence (dataset-255)

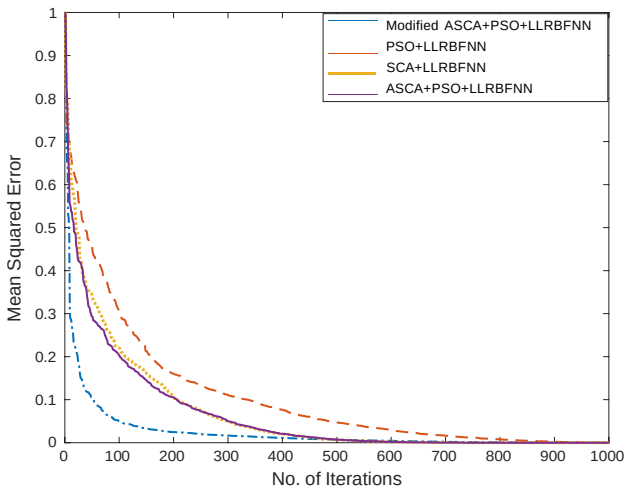


**Fig. 6** Mean squared error convergence (dataset-160)

corresponding accuracy of method over Dataset-160 during each run of cross validation is listed in Table 9. The accuracy obtained for Dataset-255 with PSO + LLRBFNN, SCA + LLRBFNN, ASCA + PSO + LLRBFNN, MASCA + PSO + LLRBFNN are 97.96%, 98.35%, 98.97%, 99.61% respectively.

The corresponding accuracy of method over Dataset-255 during each run of cross validation is listed in Table 10. Table 11 shows the fold-wise results of different performance measures at the first run in 5 × 5-fold CV procedure for Dataset-255. Nayak et al. [62] proposed Discrete ripplet-II transform and modified PSO based improved evolutionary extreme learning machine for pathological brain detection and achieved 100% accuracy in classification. In this research work, we have also tested our proposed MASCA + PSO + LLRBFNN model with features and achieved 100% accuracy in some runs with Dataset-160 and Dataset-255. The MASCA–PSO based LLRBFNN model is simple in construction and free from complex mathematical calculations in comparison to PSO based extreme learning machine. By employing feature reduction method with our proposed technique may provide better performance accuracy.

### 6.3 Classifier computational time

Computation time play an important role for evaluation of a classifier. At first, the computation time of each stage of the proposed MASCA + PSO + LLRBFNN method is recorded, and finally the average value is calculated as 7.31232 s for Dataset-255 and 8.93452 s for Dataset-160. Further the computation time for PSO + LLRBFNN, SCA + LLRBFNN and APSO + SCA + LLRBFNN for each stage has been calculated for Dataset-255 and the average value is obtained as 19.2392 s, 11.2165 s, and 10.3735 s. For Dataset-160, the computational time is obtained as 21.23147 s, 13.19823 s and 11.2931 s. It is observed that the proposed MASCA + PSO + LLRBFNN method shows faster convergence than the other mentioned algorithms. Further, the errors of the classifiers are expressed in terms of mean squared error (MSE) value shown in Fig. 5 for Dataset-255 and Fig. 6 for Dataset-160. The error is calculated for one repetition of the cross validation procedure.

The performance rate of proposed MASCA + PSO + LLRBFNN classifier depends on the convergence parameters setting. For Dataset-255, it is observed from the Fig. 5 that the proposed MASCA + PSO + LLRBFNN model takes near about 360 iterations to converge. The PSO–LLRBFNN model takes near about 780 iterations, whereas the SCA + LLRBFNN and ASCA + PSO–LLRBFNN model takes 460 and 400 iterations to converge. For Dataset-160, it is found that MASCA + PSO + LLRBFNN model takes near about 420 iterations to converge. The PSO–LLRBFNN model takes near about 800 iterations, whereas the SCA + LLRBFNN and ASCA + PSO–LLRBFNN model takes approximately 490 and 510 iterations to converge. It is found from the mean squared error results that, the accuracy in SCA + LLRBFNN and ASCA + PSO + LLRBFNN is nearly similar, but the convergence is faster in the case of MASCA + PSO + LLRBFNN classifier.

From these results and discussions, it is evident that the proposed MASCA + PSO algorithm provides superior optimized results with respect to accuracy and computational time. With the help of proposed segmentation technique, hybrid modified ASCA–PSO algorithm and statistical textural features the brain tumor images were classified into cancerous and non-cancerous tumors. The performance of

proposed technique of segmentation and textural features were found to be very useful to justify the performance of the modified ASCA–PSO based LLRBFNN classifier during training and testing.

## 7 Conclusion and future scope

In this research work, the brain magnetic resonance images are used for the purpose of segmentation and classification. To remove Rician noise and smoothen the image, an improved fast and robust FCM based segmentation technique has been employed. From the segmentation result, it is observed that the proposed improved fast and robust FCM segmentation algorithm acquires higher value of SSIM and PSNR which confirms the removal of Rician noise from magnetic resonance image. After segmentation, the texture features are extracted from magnetic resonance images using GLCM feature extraction technique. We have considered seven distinguished features for the analysis purpose. The hybrid MASCA + PSO algorithm has been proposed for updation of weights of LLRBFNN model. To justify the robustness of MASCA + PSO hybrid algorithm, six benchmark functions are considered and comparison results are presented. The extracted features are given as input to the modified ASCA + PSO based LLRBFNN classifier for classification of benign and malignant brain tumors from magnetic resonance images and compared with PSO + LLRBFNN, SCA + LLRBFNN, ASCA + PSO + LLRBFNN classifiers. The accuracy of the classifiers PSO–LLRBFNN, SCA + LLRBFNN, ASCA + PSO + LLRBFNN and MASCA + PSO + LLRBFNN for Dataset-160 and Dataset-255 shown in Table 13. The proposed classifier model has shown good potentiality in classifying the tumor into cancerous and non-cancerous brain tumors.

The results presented in this research work shows uniqueness of the model and comparison results also depict clear classification accuracies. Datast-160 and Data-255 has been collected from Harvard medical school of architecture for the purpose of segmentation and classification. The results presented using the proposed modified ASCA + PSO based LLRBFNN model is suitable automatic classification of cancerous and non-cancerous brain tumors and may help clinical diagnosis process by the radiologists or clinical experts. In the future research work, different hybrid algorithm such as BAT optimization algorithm with PSO and the harmony search for weight optimization of classifier, deep learning method, and feature reduction method with PSO–ELM for classification will be used to increase the performance accuracy. Also the advanced textures features can be considered except the mentioned texture features for the classification. Further, more efficient segmentation techniques with morphological reconstruction and membership filtering can be used for large dataset of magnetic resonance images.

## References

1. Webpage. https://consumer.healthday.com/cancer-information-5/brain-cancer-news-93/brain-cancers-both-common-and-deadl y-among-teens-young-adults-report-708339.html
2. Ding Y, Fu X (2016) Kernel-based fuzzy c-means clustering algorithm based on genetic algorithm. Neurocomputing 188:233–238. https://doi.org/10.1016/j.neucom.2015.01.106
3. Pereira DC, Ramos RP, do Nascimento MZ (2014) Segmentation and detection of breast cancer in mammograms combining wavelet analysis and genetic algorithm. Comput Methods Programs Biomed 114(1):88–101. https://doi.org/10.1016/j.cmpb.2014.01.014
4. Mahapatra D (2017) Semi-supervised learning and graph cuts for consensus based medical image segmentation. Pattern Recognit 63:700709. https://doi.org/10.1016/j.patcog.2016.09.030
5. Bahadure NB, Ray AK, Thethi HP (2017) Image analysis for MRI based brain tumor detection and feature extraction using biologically inspired BWT and SVM. Hindawi Int J Biomed Imaging 2017, Article ID 9749108. https://doi.org/10.1155/2017/9749108
6. Satheeskumaran S, Sabrigiriraj M (2014) A new LMS based noise removal and DWT based R-peak detection in ECG signal for biotelemetry applications. Natl Acad Sci Lett 37(4):341–349. https://doi.org/10.1007/s40009-014-0238-3
7. Shanmuga Priya S, Valarmathi A (2018) Efficient fuzzy c-means based multilevel image segmentation for brain tumor detection in MR images. In: Design automation for embeded system. Springer, Berlin. https://doi.org/10.1007/s10617-017-9200-1. ISSN: 1572-8080
8. Javed A, Kim YC, Khoo MCK, Ward SLD, Nayak KS (2016) Dynamic 3-D MR visualization and detection of upper airway obstruction during sleep using region-growing segmentation. IEEE Trans Biomed Eng 63(2):431–437. https://doi.org/10.1109/TBME.2015.2462750
9. Abd-Ellah MK, Awad AI, Khalaf AM, Hamed FA (2016) Design and implementation of a computer-aided diagnosis system for brain tumor classification. In: 28th international conference on microelectronics (ICM), Cairo, pp 73–76
10. Li Z, Chen J (2015) Super pixel segmentation using linear spectral clustering. In: Proceedings of the IEEE conference on computer vision and pattern recognition (CVPR), Boston, pp 1356–1363
11. Nandi AK, Basel AJ, Rui F (2015) Integrative cluster analysis in bioinformatics. Wiley, Berlin
12. Demirhan A, Güler I (2011) Combining stationary wavelet transform and self-organizing maps for brain MR image segmentation. Eng Appl Artif Intell 24:358–367. https://doi.org/10.1016/j.engappai.2010.09.008
13. Shree NV, Kumar TNR (2018) Identification and classification of brain tumor MRI images with feature extraction using DWT and probabilistic neural network. Brain Inform 5:23–30. https://doi.org/10.1007/s40708-017-0075-5
14. Chatzis SP, Varvarigou TA (2008) A fuzzy clustering approach toward hidden markov random field models for enhanced spatially constrained image segmentation. IEEE Trans Fuzzy Syst 16(5):1351–1361. https://doi.org/10.1109/TFUZZ.2008.2005008
15. Lei T, Jia X, Zhang Y, He L, Meng H, Nandi AK (2018) Significantly fast and robust fuzzy c-means clustering algorithm based on morphological reconstruction and membership filtering. IEEE Trans Fuzzy Syst 26(5):3027–3041. https://doi.org/10.1109/tfuzz.2018.2796074

16. Issa M, Hassanien AE, Oliva D, Helmi A, Ziedan I, Alzohairy A (2018) ASCA–PSO: adaptive sine cosine optimization algorithm integrated with particle swarm for pairwise local sequence alignment. Expert Syst Appl 99(1):56–70. https://doi.org/10.1016/j.eswa.2018.01.019
17. Ahmed MN, Yamany SM, Mohamed N, Farag AA, Moriarty T (2002) A modified fuzzy c-means algorithm for bias field estimation and segmentation of MRI data. IEEE Trans Med Imaging 21(3):193–199. https://doi.org/10.1109/42.996338
18. Chen S, Zhang D (2004) Robust image segmentation using FCM with spatial constraints based on new kernel-induced distance measure. IEEE Trans Syst Man Cybern B Cybern 34(4):1907–1916. https://doi.org/10.1109/tsmcb.2004.831165
19. Szilagyi L, Benyo Z, Szilagyii SM, Adam HS (2003) MR brain image segmentation using an enhanced fuzzy c-means algorithm. In: Proceeding of the 25th annual international conference of the IEEE EMBS, pp 17–21
20. Cai W, Chen S, Zhang D (2007) Fast and robust fuzzy c-means clustering algorithms incorporating local information for image segmentation. Pattern Recognit 40(3):825–838. https://doi.org/10.1016/j.patcog.2006.07.011
21. Krinidis S, Chatzis V (2010) A robust fuzzy local information c-means clustering algorithm. IEEE Trans Image Process 19(5):1328–1337. https://doi.org/10.1109/tip.2010.2040763
22. Gong M, Zhou Z, Ma J (2012) Change detection in synthetic aperture radar images based on image fusion and fuzzy clustering. IEEE Trans Image Process 21(4):2141–2151. https://doi.org/10.1109/TIP.2011.2170702
23. Gong M, Liang Y, Shi S, Ma J (2013) Fuzzy c-means clustering with local information and kernel metric for image segmentation. IEEE Trans Image Process 22(2):573–584. https://doi.org/10.1109/TIP.2012.2219547
24. Guo F, Wang X, Shen J (2016) Adaptive fuzzy c-means algorithm based on local noise detecting for image segmentation. IET Image Process 10(4):272–279. https://doi.org/10.1049/iet-ipr.2015.0236
25. Rezaei K, Agahi H (2017) Malignant and benign brain tumor segmentation and classification using SVM with weighted kernel width. Sig Image Proc Int J (SIPIJ). https://doi.org/10.5121/sipij.2017.8203
26. Torheim T, Malinen E, Kvaal K et al (2014) Classification of dynamic contrast enhanced MR images of cervical cancers using texture analysis and support vector machines. IEEE Trans Med Imaging 33(8):1648–1656. https://doi.org/10.1109/TMI.2014.2321024
27. Lang R, Zhao L, Jia K (2016) Brain tumor image segmentation based on convolution neural network. In: 2016 9th international congress on image and signal processing, biomedical engineering and informatics (CISP-BMEI), Datong, pp 1402–1406
28. Deepa SN, Arunadevi B (2013) Extreme learning machine for classification of brain tumor in 3D MR images. Informatologia 46(2):111–121. ISSN 1330-0067
29. Krishna TG, Sunitha KVN, Mishra S (2018) Detection and classification of brain tumor from MRI medical image using wavelet transform and PSO based LLRBFNN algorithm. Int J Comput Sci Eng 6(1). https://doi.org/10.26438/ijcse/v6i1.1823. E-ISSN: 2347-2693
30. Nayak PK, Mishra S, Dash PK, Bisoi Ranjeeta (2016) Comparison of modified teaching–learning-based optimization and extreme learning machine for classification of multiple power signal disturbances. Neural Comput Appl 27(7):2107–2122. https://doi.org/10.1007/s00521-015-2010-0
31. Patra A, Das S, Mishra SN, Senapati MR (2017) An adaptive local linear optimized radial basis functional neural network model for financial time series prediction. Neural Comput Appl 28(1):101–110. https://doi.org/10.1007/s00521-015-2039-0
32. Liu B, Wang L, Jin YH (2007) An effective PSO-based memetic algorithm for flow shop scheduling. IEEE Trans Syst Man Cybern B Cybern 37(1):18–27. https://doi.org/10.1109/tsmcb.2006.883272
33. Senapati MR, Vijaya I, Dash PK (2007) Rule extraction by training radial basis functional neural network with particle swarm optimization. Am J Sci 3(8):592–599. ISSN: 1549-3636
34. Yang X-S, Deb S, Fong S (2011) Accelerated particle swarm optimization and support vector machine for business optimization and applications. In: International conference on networked digital technologies, NDT 2011. Communications in computer and information science, vol 136, pp 53–66. Springer, Berlin
35. Kaur T, Saini BS, Gupta S (2016) Optimized multi threshold brain tumor image segmentation using two dimensional minimum cross entropy based on co-occurrence matrix. In: Medical imaging in clinical applications. Part of the studies in computational intelligence, vol 651. Springer, Berlin, pp 461–486. https://doi.org/10.1007/978-3-319-33793-7_20
36. Garg H (2016) A hybrid PSO–GA algorithm for constrained optimization problems. Appl Math Comput 274(1):292–305. https://doi.org/10.1016/j.amc.2015.11.001
37. de Fátima Araújoa T, Uturbey W (2013) Performance assessment of PSO, DE and hybrid PSO–DE algorithms when applied to the dispatch of generation and demand. Int J Electr Power Energy Syst 47:205–217. https://doi.org/10.1016/j.ijepes.2012.11.002
38. Santra D, Mukherjee A, Sarker K, Chatterjee D (Oct 2016) Hybrid PSO–ACO algorithm to solve economic load dispatch problem with transmission loss for small scale power system. In: 2016 international conference on intelligent control power and instrumentation (ICICPI), pp 21–23
39. Mirjalili S (2016) SCA: a sine cosine algorithm for solving optimization problems. Knowl Based Syst 96:120–133. https://doi.org/10.1016/j.knosys.2015.12.022
40. Tasnin W, Saikia LC (2018) Maiden application of an sine–cosine algorithm optimised FO cascade controller in automatic generation control of multi-area thermal system incorporating dish-Stirling solar and geothermal power plants. IET Renew Power Gener 12(5):585–597. https://doi.org/10.1049/iet-rpg.2017.0063
41. Nenavath H, Jatoth RK, Das S (2018) A synergy of the sine–cosine algorithm and particle swarm optimizer for improved global optimization and object tracking. Swarm Evol Comput. https://doi.org/10.1016/j.swevo.2018.02.011
42. Gonçalves H, Gonçalves JA, Corte-Real L (2011) HAIRIS: a method for automatic image registration through histogram-based image segmentation. IEEE Trans Image Process 20(3):776–789. https://doi.org/10.1109/TIP.2010.2076298
43. Jamil M, Yang X-S (2013) A literature survey of benchmark functions for global optimization problems. Int J Math Model Numer Optim 4(2):150–194. https://doi.org/10.1504/IJMMNO.2013.055204
44. Smith TM, Bonacuse P, Sosa J, Kulis M, Evans L (2018) A quantifiable and automated volume fraction characterization technique for secondary and tertiary γ′ precipitates in Ni-based super alloys. Mater Charact 140:86–94. https://doi.org/10.1016/j.matchar.2018.03.051
45. Pal C, Das P, Chakrabarti A, Ghosh R (2017) Rician noise removal in magnitude MRI images using efficient anisotropic diffusion filtering. Int J Imaging Syst Technol 27(3):248–264. https://doi.org/10.1002/ima.22230
46. Aja-Fernandez S, Alberola-Lopez C, Westin C-F (2008) Noise and signal estimation in magnitude MRI and Rician distributed images: A LMMSE approach. IEEE Trans Image Process 17(8):1383–1398. https://doi.org/10.1109/tip.2008.925382
47. Dataset: Webpage of Medical School of Harvard University. www.med.harvard.edu/AANLIB/home.html

48. Cocosco CA, Kollokian V, Kwan RK-S, Evans AC (2011). BrainWeb: online interface to a 3D MRI simulated brain database (Online). http://www.bic.mni.mcgill.ca/brainweb
49. Wang Z, Bovik AC, Sheikh HR, Simoncelli EP (2004) Image quality assessment: from error visibility to structural similarity. IEEE Trans Image Process 13(4):600–612. https://doi.org/10.1109/TIP.2003.819861
50. Aja-Fernandez S, San-José-Estépar R, Alberola-Lopez C, Westin C (Sept 2006) Image quality assessment based on local variance. In: Proceeding of the 28th IEEE EMBS, New York, pp 4815–4818
51. Nenavatha H, Jatotha RK, Das S (2018) A synergy of the sine–cosine algorithm and particle swarm optimizer for improved global optimization and object tracking. Swarm Evol Comput 43:1–30. https://doi.org/10.1016/j.swevo.2018.02.011
52. Mirjalili S, Gandomi AH, Mirjalili SZ, Saremi S, Faris H, Mirjalili SM (2017) Slap swarm algorithm: a bio-inspired optimizer for engineering design problems. Adv Eng Softw 114:163–191. https://doi.org/10.1016/j.advengsoft.2017.07.002
53. Mirjalili S, Mirjalili SM, Lewis A (2014) Gary wolf optimizer. Adv Eng Softw 69:46–61. https://doi.org/10.1016/j.advengsoft.2013.12.007
54. Mirjalili S, Lewis A (2016) The whale optimization algorithm. Adv Eng Softw 95:51–67. https://doi.org/10.1016/j.advengsoft.2016.01.008
55. Mirjalili S (2015) Mouth –flame optimization algorithm: a novel nature-inspired heuristic paradigm. Knowl Based Syst 89:228–249. https://doi.org/10.1016/j.knosys.2015.07.006
56. Xu Y, Fan P, Yuan L (2013) A simple and efficient artificial bee colony algorithm. Math Probl Eng 2013:1–9, Article ID 526315, Hindawi. http://dx.doi.org/10.1155/2013/526315
57. Mahesh KM, Renjit JA (2018) Evolutionary intelligence for brain tumor recognition from MRI images: a critical study and review. Evol Intell. https://doi.org/10.1007/s12065-018-0156-2
58. Nayak DR, Dash R, Majhi B (2016) Brain MR image classification using two-dimensional discrete wavelet transform and AdaBoost with random forests. Neurocomputing 117:188–197. https://doi.org/10.1016/j.neucom.2015.11.034i
59. Mohana G, Subashini MM (2018) MRI based medical image analysis: survey on brain tumor grade classification. Biomed Signal Process Control 39:139–161
60. Mohanaiah P, Sathyanarayana P, GuruKumar L (2013) Image texture feature extraction using GLCM approach. Int J Sci Res Publ 3(5):1
61. Das S, Chowdhury M, Kundu MK (2013) Brain MR image classification using multiscale geometric analysis of ripplet. Prog Electromagn Res 137:1–17. https://doi.org/10.2528/PIER13010105
62. Nayak DR, Dash R, Majhi B (2017) Discrete ripplet-II transform and modified PSO based improved evolutionary extreme learning machine for pathological brain detection. Neurocomputing. https://doi.org/10.1016/j.neucom.2017.12.030